Chinese Chemical Letters 35 (2024) 108504

Contents lists available at ScienceDirect

Chinese Chemical Letters

journal homepage: www.elsevier.com/locate/cclet

High-throughput fluorescent screening of thioredoxin reductase inhibitors to inhibit *Mycobacterium tuberculosis*

Fei Yan[a,1], Xin Zhao[b,1], Ruibo Li[c], Xiuyan Han[a,*], Qiulong Yan[a], Lei Feng[a,d,*], Xiulan Xin[e], Jingnan Cui[b], Xiaochi Ma[a,c,*]

[a] *Second Affiliated Hospital, Dalian Medical University, Dalian 116044, China*
[b] *State Key Laboratory of Fine Chemicals, Dalian University of Technology, Dalian 116024, China*
[c] *Jiangsu Key Laboratory of New Drug Research and Clinical Pharmacy, Xuzhou Medical University, Xuzhou 221004, China*
[d] *School of Chemistry and Chemical Engineering, Henan Normal University, Xinxiang 453007, China*
[e] *College of Bioengineering, Beijing Polytechnic, Beijing 100029, China*

A R T I C L E I N F O

Article history:
Received 7 March 2023
Revised 21 April 2023
Accepted 23 April 2023
Available online 28 April 2023

Keywords:
Thioredoxin reductase
NIR fluorescent probe
Fluorescence imaging
High-throughput screening inhibitors
Inhibit *Mycobacterium tuberculosis*

A B S T R A C T

Tuberculosis (TB) is a chronic infectious disease, which is caused by the pathogen *Mycobacterium tuberculosis* (Mtb) and reemerged as a global health risk with a significant proportion of multi-drug resistant and extensively drug resistant TB cases. It is very urgent to find some novel high-confidence drug targets in Mtb for discovering the effective anti-TB agents. Thioredoxin reductase (TrxR) has been identified to be a highly viable target for anti-TB drugs for its important role in protecting the pathogen from thiol-specific oxidizing stress, regulating intracellular dithiol/disulfide homeostasis and DNA replication and repair. In the present work, a near-infrared (NIR) fluorescent probe **DDAT** was developed for the detection of TrxR activity and used to high-throughput screen the TrxR inhibitors from natural products. Two screened TrxR inhibitors from *Sappan Lignum* and microbial metabolites that were further used to inhibit *Mycobacterium tuberculosis*. All the results indicate that **DDAT** is a practical fluorescent molecular tool for the discovery of potential anti-TB drugs.

Tuberculosis (TB) is a chronic infectious disease, which is caused by the pathogen *Mycobacterium tuberculosis* (Mtb) and spread by expelling the pathogen into air from TB patients [1]. The World Health Organization released that “End TB Strategy” aims to reduce TB deaths by 90% and TB incidence by 80% by 2030, compared to the 2015 baseline. However, the progress in tackling TB has reversed due to the Corona Virus Disease 2019 (COVID-19) pandemic. Today, TB is still the second most deadly infectious disease after COVID-19, responsible for about 1.6 million deaths in 2021 [2]. In addition, TB reemerged as a global health risk with a signification proportion of multi-drug resistant and extensively drug resistant TB cases that the resistant pathogen is not sensitive to currently available anti-TB drugs. Consequently, there is increased need to find novel high-confidence drug targets in Mtb for discovering effective anti-TB agents.

Mtb has an ingenious molecular mechanism to resist and adapt redox stresses in host cells during persistent infection by altering Mtb signal transduction, transcription and translation and drug resistance [3]. Among them, the essential thiol-reducing enzyme thioredoxin reductase (TrxR) in Mtb forms an antioxidant system with three thioredoxin proteins and nicotinamide adenine dinucleotide phosphate (NADPH) to protect the pathogen from thiol-specific oxidizing stress and regulate intracellular dithiol/disulfide homeostasis [4,5], various biological processes in the pathogen cell are also regulated by TrxR, such as defense against hydrogen peroxide [6], response to hypoxia [7] and protection the pathogen in macrophages [8]. In addition, TrxR has been proven to play an important role in the catalytic mechanism of ribonucleotide reductase, which is involved in DNA replication and repair [9]. Therefore, TrxR has been identified to be a highly viable target for anti-TB drugs [10–12] as well as closely connected to drug-resistance proteins RecA and two cytochromes in Mtb [13].

With the advantages of high efficiency and sensitivity, high-throughput screening systems based on fluorescence technology have been paid more and more attention in environmental monitoring, physiological process detection and the discovery of lead compounds [14–19]. Up to now, several fluorescent probes have been reported to measure the activity of TrxR in tumor and in-

* Corresponding authors.
E-mail addresses: hanxiuy@yeah.com (X. Han), leifeng@dmu.edu.cn (L. Feng), maxc1978@163.com (X. Ma).
[1] These authors contributed equally to this work.

https://doi.org/10.1016/j.cclet.2023.108504

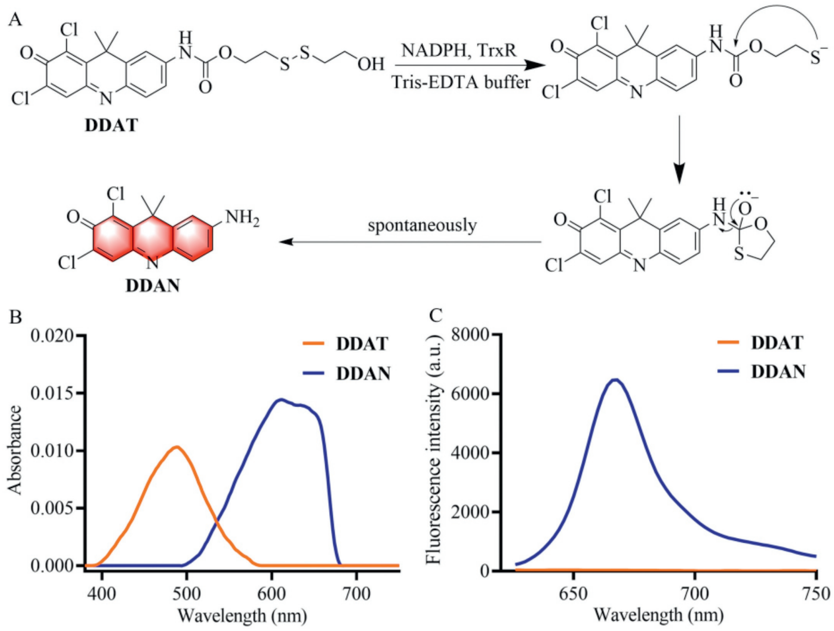

Fig. 1. (A) Illustration of the enzymatic catalysis progress of **DDAT** mediated by TrxR. (B) Absorbance of **DDAT** and **DDAN**. (C) Fluorescence spectra of **DDAT** and **DDAN**.

flammatory disease [20–31], while few probes for TrxR were used in TB treatment.

Herein, a near-infrared (NIR) fluorescent probe **DDAT** was developed for the rapid and sensitive detection of TrxR activity, and used to high-throughput screen TrxR inhibitors from natural products that were further used to inhibit Mtb. Two screened TrxR inhibitors form herbal medicines and microbial metabolites displayed potent anti-TB activity through the disruption of DNA synthesis and redox imbalance in Mtb, which means that **DDAT** is a practical fluorescent molecular tool for the discovery of new anti-TB drugs.

DDAT was designed by introducing TrxR's recognition group disulfide bond into the NIR fluorophore **DDAN** through amide bond according to the synthetic route in Scheme S1 (Supporting information), and the nuclear magnetic resonance spectroscopy (NMR) and high resolution mass spectroscopy (HRMS) data are provided as Figs. S1−S3 (Supporting information). TrxR can reduce disulfide bond to produce sulfhydryl group, which further spontaneously attack amide bond to hydrolyze and release **DDAN** (Fig. 1A), which is accompanied by the redshift of absorption and the "Off-On" change of NIR fluorescence signal (Figs. 1B and C). These results indicate that **DDAT** could be used as a NIR fluorescent probe to detect TrxR activity.

Then the effects of pH and temperature on the reaction system were investigated. As shown in Fig. S4A (Supporting information), **DDAT** had good stability in the range of pH 3.0−9.0, and the product **DDAN** maintained stable fluorescence intensity in the range of pH 5.0−9.0, indicating that the probe had good stability under physiological conditions. Subsequently, the influence of temperature on the catalytic efficiency of TrxR was investigated. As can be seen in Fig. S4B (Supporting information), although the catalytic efficiency of TrxR was the highest at 42 °C, the incubation temperature of 37 °C was finally selected considering physiological conditions. The stability of **DDAT** is also investigated in a variety of endogenous substances (tryptophan, serine, glutamine, glycine, arginine, lysine, glutamic acid, cysteine, glutathione and myristic acid) and common ions (K^+, Na^+, Mg^{2+}, Ca^{2+}, Ba^{2+}, Zn^{2+}, Cu^{2+}, Ni^{2+}, Sn^{4+}, Mn^{2+}, CO_3^{2-}, SO_4^{2-}, Fe^{2+}, Fe^{3+}, Cl^-, NO_2^-, HPO_4^{2-} and $H_2PO_4^-$). The results showed that the fluorescence intensity of **DDAT** was not affected by the interference of endogenous substances and common ions, which showed excellent stability (Fig. S5 in Supporting information).

Next, the selectivity of **DDAT** toward TrxR was also investigated. The recombinant Mtb TrxR expressed in *E. coli* BL21 (DE3) according to the methods in Supporting information (Figs. S6–S9). Fig. 2A showed that only TrxR elicited a dramatic increase in the fluorescence intensity at 666 nm, while other enzymes including carboxylesterases (CEs1b, CEs2), β-glucosidase (β-Glc), elastase, acetaldehyde dehydrogenase (ALDH), nitroreductase (NTR), human serum albumin (HSA), horseradish peroxidase (HRP), *N*-acetyl-β-D-glucosaminidase (NAG), β-glucuronidase (β-Glu), lipase, carbonic anhydrase (CA), acetylcholinesterase (AchE), butylcholinesterase (BchE), alcohol dehydrogenase (ADH) and dipeptidyl peptidase-4 (DPP4) led to negligible changes in fluorescence intensity. To further investigate the selectivity, the inhibition assays were conducted in the lysates of wild type Mtb H37Ra by using a series of inhibitors. As can be seen in Fig. 2B, only ebselen, a selective inhibitor of TrxR [32], can significantly inhibit the catalytic process of **DDAT** metabolized by TrxR, other types of inhibitors such as bis(4-nitrophenyl)phosphate (BNPP, inhibitor of carboxylesterases) [33], sivelestat sodium (inhibitor of elastase) [34], rivastigmine (a selective inhibitor of AchE) [35], and dicoumarin (inhibitor of nitroreductase) [36] have no effect on the catalytic process. These results further confirm the specificity of **DDAT** toward TrxR.

To monitor the real activity of the target enzyme quantitatively, the linear fluorescence intensity response toward enzyme concentration is very essential. As shown in Figs. 2C and D, the fluorescence signal gradually enhanced with increasing TrxR, and the fluorescence intensity at 666 nm and TrxR concentrations in the range from 0 to 21 µg/mL showed good linear relationship (limit of detection = 0.22 µg/mL, 3 σ/k). To elucidate the binding interactions between **DDAT** and TrxR, molecular docking simulation was performed. The binding energy is −7.4 kcal/mol, indicating that **DDAT** can bind to the protein spontaneously. There were hydrogen bonds, π-π stacking, π-alkyl, and van der Waals interactions observed (Fig. S10 in Supporting information). **DDAT** may form hydrogen bond interactions with the protein's LYS394 and ASN388, and its hydrophobic functional groups may form hydrophobic interactions with the protein's PHE71, PHE256, and ALA241. The benzene

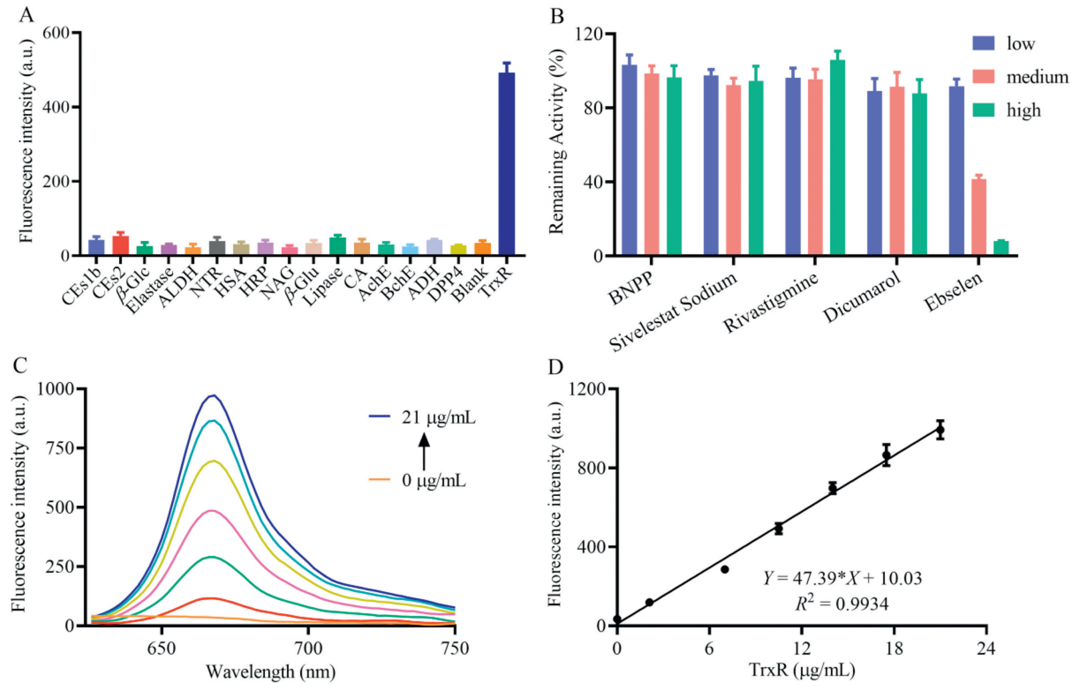

Fig. 2. (A) Interference of various enzymes on the fluorescence intensity of **DDAT**. (B) Interference of different inhibitors on the reaction of **DDAT** mediated by TrxR. (C) Fluorescence response of **DDAT** toward TrxR with different concentrations. (D) Linear relationship between fluorescence intensity at 666 nm and TrxR concentrations (λ_{ex} = 600 nm, λ_{em} = 666 nm).

ring in the compound interacts with the benzene ring in the PHE71 and PHE256 amino acids of the protein to form a π-stacking (perpendicular) interaction, and the halogen atom in the compound interacts with ARG263 of the protein to form a halogen bond. All these results indicate that **DDAT** is a practical molecular tool that could be used to detect the activity of TrxR selectively and sensitively in complex biosystems.

By virtue of the superior performance of **DDAT**, a fluorescence-based high-throughput screening platform for TrxR inhibitors from 260 kinds of herbal medicines and 180 kinds of microbial metabolites was constructed. As can be seen in Fig. 3A, *Sappan Lignum* displayed the strongest inhibitory effect on TrxR (17.96% residual activity). *Forsythiae Fructus, Phellodendri Chinensis Cortex* and *Myrrha* showed moderate inhibitory activity (40% to 60% residual activity) against TrxR. *Carthami Flos, Vaccariae Semen* and *Cimicifugae Rhizoma* showed weak inhibitory effects on TrxR (80% to 100% residual activity). Then, 11 fractions from the *Sappan Lignum* were collected (Fig. 3B), and the inhibitory effect of the fractions toward TrxR was evaluated by microplate reader. As Fig. 3C bar chart showed, Fr.3 showed the strongest inhibitory effect on TrxR, and the main active component of Fr.3 was Brazilin (Brz) that was identified by ^{1}H NMR, ^{13}C NMR and HRMS (Fig. 4A, Figs. S11–S13 in Supporting information). In addition, the inhibitory effect was also evaluated visually by fluorescence scanning imager (inset of Fig. 3C), and the two methods are in good agreement (Fig. S14 in Supporting information).

The inhibitory effect of Brz on TrxR was further evaluated by **DDAT**, the half-inhibitory concentration (IC_{50} value) was calculated to be 3.63 μmol/L (Fig. 4B) and the binding energy is −7.1 kcal/mol, indicating that Brz can bind to TrxR spontaneously. There were hydrogen bonds, π-π stacking, π-alkyl, and van der Waals interactions observed (Figs. 4C–E). Brz may form hydrogen bond interactions with the protein's SER1 and SER386, and its hydrophobic functional groups may form hydrophobic interactions with the protein's ALA69, PHE71, and PHE146. These results indicated that Brz had good affinity with TrxR.

In addition, the fluorescence-based high-throughput screening platform was also used to discover TrxR inhibitors from 180 kinds of microbial metabolites, as shown in Fig. S15 (Supporting information), gliotoxin (GTX), one of the mycotoxins produced by *Aspergillus fumigatus* showed the strongest inhibitory activity against TrxR with the IC_{50} value 1.85 μmol/L (Fig. S16 in Supporting information). Autodock-vina was used for molecular docking, and the binding energy of GTX and TrxR was −7.5 kcal/mol, indicating that the target had strong binding ability with GTX that could effectively bind to the active pocket of TrxR protein, and could spontaneously generate hydrogen bonding and hydrophobic interaction with the protein-binding pocket. Subsequently, by analyzing the three-dimensional interaction, it was found that GTX could form hydrogen bond interaction with SER47 and ARG253, and the hydrogen bond distances were 2.99 Å and 2.80 Å. Additionally, GTX was able to form hydrophobic interactions with THR54, TYR128, and ALA126 of the protein. These interactions promote the binding of GTX to the active pockets of TrxR to form complexes that exert inhibitory effect.

Then, the fluorescence imaging ability of **DDAT** was investigated, as shown in Fig. 5A, obvious fluorescence signal was observed after incubation with **DDAT**, while the fluorescence signal was significantly weakened when pre-incubated with the TrxR specific inhibitor ebselen. These results indicated that the fluorescence signal was generated from **DDAT** mediated by TrxR. Subsequently, flow cytometry was used to evaluate the ability of **DDAT** in detecting TrxR activity. As shown in Fig. 5B, right shift represented the enhancement of fluorescence signal, and the fluorescence signal of **DDAT** treatment group (CON) was significantly right shift compared with blank group (Blank). The right-shift amplitude of fluorescence signal in ebselen treatment group was smaller than that in probe treatment group. Besides, GTX can significantly inhibit the fluorescence signal of **DDAT** mediated by TrxR in Mtb H37Ra (Fig. S17 in Supporting information). These results indicate that **DDAT** is highly sensitive to the endogenous TrxR of Mtb and can be used to detect the activity of TrxR in complex biosystems.

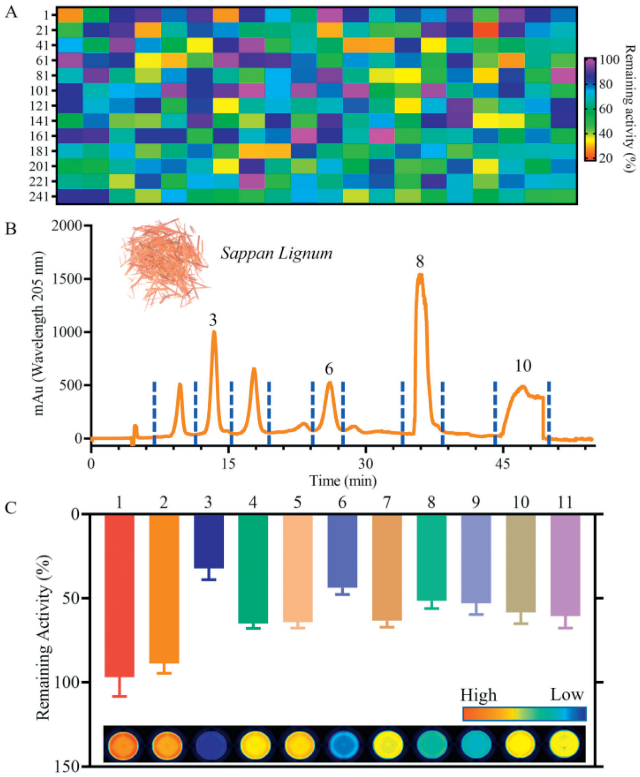

Fig. 3. (A) The heat map of inhibitory effect of 260 kinds of herbal medicines toward TrxR by using **DDAT**. (B) Fractions of *Sappan Lignum*. (C) The remaining activity of TrxR measured using **DDAT** by microplate reader (bar chart), and fluorescence images of remaining TrxR activity based on the relative intensity (inset).

The drug sensitivity test of Mtb H37Ra was carried out according to the AlamarBlue method. It could be determined from Fig. 6A that the minimum inhibitory concentration (MIC) of Brz on Mtb H37Ra was 60 μmol/L, and the MIC of GTX was 50 nmol/L (Fig. 6B), indicating that the inhibitors Brz and GTX have good antibacterial effect on Mtb H37Ra, and the effect of GTX is particularly obvious. Next, GTX was further used to evaluate the effect on the growth rate of Mtb H37Ra. As shown in Fig. S18 (Supporting information), GTX could significantly inhibit the growth of Mtb H37Ra, thus proving the growth necessity of TrxR for Mtb. The ability of propidium iodide (PI) to pass through damaged cell membranes and bind to DNA can determine whether a cell is broken. It can be seen from the PI staining results that almost no red fluorescence signal can be observed in the wild type Mtb H37Ra, and the red fluorescence signal of PI after binding with DNA could be obviously observed in the GTX treated group (Fig. S19 in Supporting information). These results indicated that GTX inhibited the activity and function of TrxR, thereby destroying the integrity of cell wall and eventually causing cell damage. The inhibitory effect of inhibitors mentioned above were also analyzed by scanning electron microscope. As shown in Fig. 6C, the wild type bacteria had a regular appearance, showing a rod shape with a flat surface, while GTX and Brz treatment groups showed different length and surface shrinkage and uneven (Figs. 6D and E). All these results indicate that the screened TrxR inhibitors Brz and GTX destroy the integrity of cell wall through inhibiting the normal physiological function of TrxR that has good anti-TB effect.

In summary, a NIR fluorescent probe named **DDAT** was designed and developed for the detection of TrxR, which showed highly selectivity and sensitivity toward TrxR, and could be used to monitor the activity of TrxR quantitatively in complex biosystems. In addition, a fluorescence-based high-throughput screening platform for TrxR inhibitors was established based on **DDAT**, and *Sappan Lignum* from herbal medicines and gliotoxin from microbial metabolites showed strong inhibitory activity against TrxR, the main active component of *Sappan Lignum* was further identified as Brazilin. These two screened inhibitors displayed good anti-TB effect by destroying the integrity of cell wall and eventually causing cell damage that may be used as anti-TB lead compounds, which means that **DDAT** is a practical fluorescent molecular tool for the discovery of potential anti-TB agents.

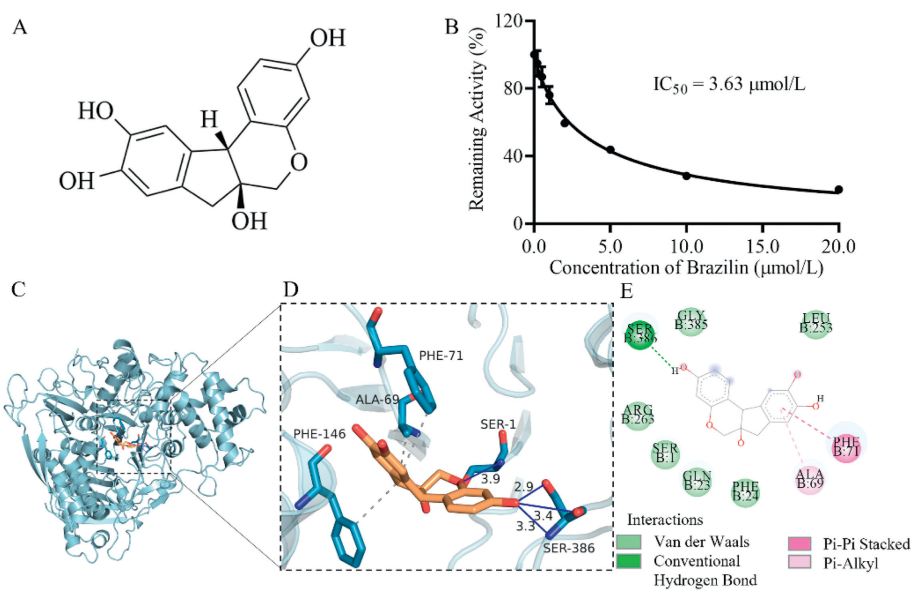

Fig. 4. (A) Structure of Brz; (B) the inhibition IC_{50} curve of Brz toward TrxR; (C) *in silico* docking analysis for **DDAT** and TrxR protein; (D) a detailed view of (C); (E) the possible key binding of the amino acids' residues.

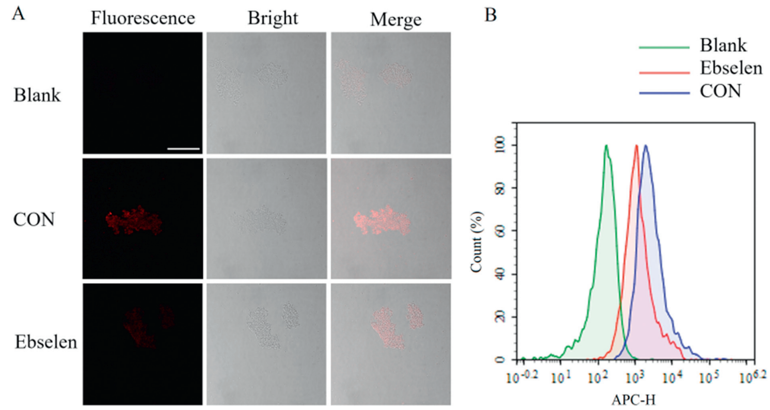

Fig. 5. (A) Fluorescence imaging of Mtb H37Ra incubated with **DDAT** (CON) and pre-incubated with ebselen. (B) Flow Cytometric analysis of Mtb H37Ra (green) with **DDAT** (blue) or ebselen and **DDAT** (red). Scale bar: 50 µm.

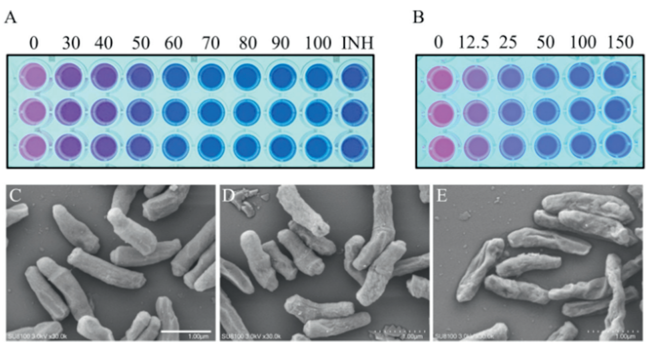

Fig. 6. The inhibitory effect of Brz (µmol/L) (A) and GTX (nmol/L) (B) on Mtb H37Ra was measured by AlamarBlue method. The scanning electron microscope of Mtb H37Ra after treatment with or without inhibitors. (C) Wild type Mtb H37Ra; (D) with GTX; (E) with Brz. Scale bar: 1 µm in C, D, E.

Declaration of competing interest

The authors declare that they have no known competing financial interests or personal relationships that could have appeared to influence the work reported in this paper.

Acknowledgments

The authors thank the National Natural Science Foundation of China (Nos. 81930112 and 82225048), Open Research Fund of the School of Chemistry and Chemical Engineering, Henan Normal University for support (No. 2021YB07), and Research on National Reference Material and Product Development of Natural Products (No. SG030801, Beijing Polytechnic).

Supplementary materials

Supplementary material associated with this article can be found, in the online version, at doi:10.1016/j.cclet.2023.108504.

References

[1] D.T. Hoagland, J. Liu, R.B. Lee, et al., Adv. Drug Deliv. Rev. 102 (2016) 55–72.
[2] World Health Organization, Global tuberculosis report (accessed 6 February 2023). https://www.who.int/teams/global-tuberculosis-programme/data.
[3] N.M. Parrish, J.D. Dick, W.R. Bishai, Trends Microbiol. 6 (1998) 107–112.
[4] Z. Zhang, P.J. Hillas, P.R. Ortiz de Montellano, Arch. Biochem. Biophys. 363 (1999) 19–26.
[5] M. Akif, R. Chauhan, S.C. Mande, Acta Crystallogr. D 60 (2004) 777–779.
[6] T. Takemoto, Q.M. Zhang, S. Yonei, Free Radic. Biol. Med. 24 (1998) 556–562.
[7] J. Starck, G. Kallenius, B.I. Marklund, et al., Microbiology 150 (2004) 3821–3829.
[8] J.S. Schorey, M.C. Carroll, E.J. Brown, Science 277 (1997) 1091–1093.
[9] A. Holmgren, R. Sengupta, Free Radic. Biol. Med. 49 (2010) 1617–1628.
[10] O. Koch, T. Jager, K. Heller, et al., J. Med. Chem. 56 (2013) 4849–4859.
[11] J. Lu, A. Vlamis-Gardikas, K. Kandasamy, et al., FASEB J. 27 (2013) 1394–1403.
[12] J. Lu, A. Holmgren, Free Radic. Biol. Med. 66 (2014) 75–87.
[13] K. Raman, K. Yeturu, N. Chandra, BMC Syst. Biol. 2 (2008) 109.
[14] F. Yan, J. Cui, C. Wang, et al., Chin. Chem. Lett. 33 (2022) 4219–4222.
[15] H. Zhang, J. Fan, J. Wang, et al., J. Am. Chem. Soc. 135 (2013) 11663–11669.
[16] Y. Zhang, W. Zhou, N. Xu, et al., Chin. Chem. Lett. 34 (2023) 107472.
[17] F. Yan, S. He, X. Han, et al., Biosens. Bioelectron. 216 (2022) 114606.
[18] H. Li, H. Kim, F. Xu, et al., Chem. Soc. Rev. 51 (2022) 1795–1835.
[19] H. Zhang, Y. Xu, H. Li, et al., Chem 8 (2022) 287–295.
[20] M.H. Lee, H.M. Jeon, J.H. Han, et al., J. Am. Chem. Soc. 136 (2014) 8430–8437.
[21] X. Li, B. Zhang, C. Yan, et al., Nat. Commun. 10 (2019) 2745.
[22] L. Zhang, D. Duan, Y. Liu, et al., J. Am. Chem. Soc. 136 (2014) 226–233.
[23] M.H. Lee, J.H. Han, J.H. Lee, et al., J. Am. Chem. Soc. 134 (2012) 17314–17319.
[24] T.J. Mafireyi, M. Laws, J.W. Bassett, et al., Angew. Chem. Int. Ed. 59 (2020) 15147–15151.
[25] H. Ma, J. Zhang, Z. Zhang, et al., Chem. Commun. 52 (2016) 12060–12063.
[26] X. Zuo, Y. Zhao, J. Zhao, et al., Analyst 147 (2022) 834–840.
[27] Y. Zhao, X. Zuo, S. Liu, et al., Antioxidants 11 (2022) 377.
[28] R. Liu, D. Shi, J. Zhang, et al., Toxicol. Appl. Pharmacol. 370 (2019) 106–116.
[29] J. Li, Q. Qiao, Y. Ruan, et al., Chin. Chem. Lett. 34 (2023) 108266.
[30] H. Gong, Y. Zhang, Y. Gao, et al., Chin. Chem. Lett. 34 (2023) 108329.
[31] X. Zhang, F. Yang, T. Ren, et al., Chin. Chem. Lett. 34 (2023) 107835.
[32] R. Zhao, H. Masayasu, A. Holmgren, Proc. Natl. Acad. Sci. U. S. A. 99 (2002) 8579–8584.
[33] J.G. Slatter, P. Su, J.P. Sams, et al., Drug Metab. Dispos. 25 (1997) 1157–1164.
[34] E. Polverino, E. Rosales-Mayor, G.E. Dale, et al., Chest 152 (2017) 249–262.
[35] T.H. Ferreira-Vieira, I.M. Guimaraes, F.R. Silva, et al., Curr. Neuropharmacol. 14 (2016) 101–115.
[36] E. Johansson, G.N. Parkinson, W.A. Denny, et al., J. Med. Chem. 46 (2003) 4009–4020.